Bio-mimetic hollow scaffolds for long bone replacement

Bert Müller*[a,b], Hans Deyhle[a,b], Fabienne C. Fierz[a], Stephan H. Irsen[c], Jin Yu Yoon[a,b], Shpend Mushkolaj[a], Oliver Boss[a], Elke Vorndran[d], Uwe Gbureck[d], Özer Degistirici[c,e], Michael Thie[c,f], Barbara Leukers[c,g], Felix Beckmann[h], Frank Witte[i]
[a]Biomaterials Science Center, University of Basel, c/o University Hospital, 4031 Basel, Switzerland;
[b]School of Dental Medicine, University of Basel, Hebelstrasse 3, 4056 Basel, Switzerland;
[c]caesar Research Center, Ludwig-Erhard-Allee 2, 53175 Bonn, Germany;
[d]Department for Functional Materials in Medicine and Dentistry, University of Würzburg, Pleicherwall 2, D-97070 Würzburg, Germany
[e]University Hospital Düsseldorf, Moorenstr. 5, 40225 Düsseldorf, Germany
[f]Institute of Anatomy and Clinical Morphology, University Witten-Herdecke, Alfred-Herrhausen-Str. 50, 58448 Witten, Germany
[g]Lohmann & Rauscher GmbH & Co. KG, Irlicher Str. 55, 56567 Neuwied, Germany
[h]GKSS Research Center, Max-Planck-Str. 1, 21502 Geesthacht, Germany
[i]Hannover Medical School, Anna-von-Borries-Str. 1-7, 30625 Hannover, Germany

ABSTRACT

The tissue engineering focuses on synthesis or regeneration of tissues and organs. The hierarchical structure of nearly all porous scaffolds on the macro, micro- and nanometer scales resembles that of engineering foams dedicated for technical applications, but differ from the complex architecture of long bone. A major obstacle of scaffold architecture in tissue regeneration is the limited cell infiltration as the result of the engineering approaches. The biological cells seeded on the three-dimensional constructs are finally only located on the scaffold's periphery. This paper reports on the successful realization of calcium phosphate scaffolds with an anatomical architecture similar to long bones. Two base materials, namely nano-porous spray-dried hydroxyapatite hollow spheres and tri-calcium phosphate powder, were used to manufacture cylindrically shaped, 3D-printed scaffolds with micro-passages and one central macro-canal following the general architecture of long bones. The macro-canal is built for the surgical placement of nerves or larger blood vessels. The micro-passages allow for cell migration and capillary formation through the entire scaffold. Finally, the nano-porosity is essential for the molecule transport crucial for signaling, any cell nutrition and waste removal.

Keywords: bone architecture, microstructure, nanostructure, tomography, 3D printing, hydroxyapatite, tri-calcium phosphate, cyto-compatibility, synchrotron radiation

1. INTRODUCTION

Tissue engineering focuses on the synthesis and/or the regeneration of tissues and organs. Here, a synthetic porous scaffold, or matrix, which mimics the extra-cellular matrix properties, allows for cell attachment, proliferation, migration, and function. The macro-, micro- and nano-structural elements of many porous scaffolds resemble that of engineering foams, but do not follow the architecture of mechanically loaded long bone. Consequently, the seeded biological cells such as osteoblasts are primarily located on the scaffold's periphery and are organized in cell clusters inhomogeneously distributed within the engineered scaffold. Nano-porous spray-dried hydroxyapatite hollow spheres can be used to realize 3D-printed scaffolds with micro-passages and macro-canals following the general architecture of long bones. The macro-canals are introduced to allow the surgeon to place nerves or larger blood vessels inside the scaffold as can be found in the cancellous bone (spongy bone). The micro-passages should allow for the *in vitro* and *in vivo* cell migration and capillary formation through the entire scaffold, especially important at the periphery, where the architecture should become similar to the cortical bone (corticalis), which provides the necessary mechanical stability of the cell-seeded scaffold. The nano-porosity, finally, is essential for the molecule transport fundamental for signaling, any cell nutrition and waste removal.

*bert.mueller@unibas.ch, www.bmc.unibas.ch

Biomimetics and Bioinspiration, edited by Raúl J. Martín-Palma, Akhlesh Lakhtakia, Proc. of SPIE Vol. 7401, 74010D · © 2009 SPIE · CCC code: 0277-786X/09/$18 · doi: 10.1117/12.825487

For the 3D powder printing of calcium phosphate scaffolds organic or inorganic binders are sprayed onto a horizontal powder bed. The fluid locally binds the ceramic particles thanks to adhesive forces or a hydraulic cement setting reaction. Subsequently, a thin powder layer is applied on top. The entire process is repeated until the fabrication of the construct is finalized. 3D powder printing, a commercially established process, is based on gypsum or starch powders for technical applications [1, 2]. The binders were adapted to (bio)materials using poly-lactic acid (PLA) with chloroform [3] and ethanol-acetone mixtures [4]. Bare calcium phosphate powders [5-7] or powders with polymeric additives [8, 9] were combined with polymeric or acidic binder solutions. Inorganic binder solutions allow the hydraulic setting of the powder matrix as known from self-setting calcium phosphate cements [10, 11]. For example, the phosphoric acid solution reacts with tri-calcium phosphate powder to become di-calcium phosphate di-hydrate.

Having evaluated the hydroxy-apatite scaffold morphology in detail [12], the present communication provides additional information on the cyto-compatibility and mechanical properties of the cylindrically shaped ceramic bone scaffolds. For this purpose, the scaffolds were seeded with human multi-potent dental neural crest-derived progenitor cells (dNC-PCs). The mechanically fragile hydroxy-apatite scaffolds are compared with specimens printed from alpha tri-calcium phosphate powder and diluted phosphoric acid solution. This route allows fabricating low-temperature brushite scaffolds.

2. MATERIALS AND METHODS

2.1 Biologically inspired scaffold design

Calcium phosphate scaffolds labeled Design A, B and C were proposed for pixel- and layer-wise fabrication. The cubic voxels should correspond to a length of 240 µm. The scaffolds consist of 15 alternating double-layers corresponding to the two circular microstructures as demonstrated in the scheme of Figure 1. All three designs contain a millimeter-wide axial channel with a minimal width of 4 voxels. It is connected to perpendicularly arranged micro-channels. In the red-colored layer of Figure 1 one detects these pores, 8 for Design A and 12 for Designs B and C. The cylindrical shape was not only chosen to mimic the hollow bone structure but also to obtain comparable total X-ray absorption for the tomography measurements in different directions of the horizontal plane.

2.2 3D-printing of calcium phosphate scaffolds

Hydroxy apatite scaffolds of the three designs represented in Figure 1 were fabricated layer-by-layer by means of 3D printing, which belongs to the rapid prototyping techniques. The unique 3D printer was detailed described earlier [9]. A modified spray-dryer served for the production of the bioceramic granulates from a water-based slurry [13]. The mean particle size of the porous hydroxy apatite granules corresponded to 22 µm. An aqueous polymer solution bonded the granules in the 3D printer at predefined pixels in each printing layer. The cubic voxel size of 240 µm corresponds to the printer resolution of 106 dpi. The heat treatment of the printed green bodies included the removal of the polymeric binder at a temperature of 450 °C and the subsequent sintering at a temperature of 1250 °C for a period of 2 h to reach a tolerable mechanical stability for the handling.

The synthesis of the tri-calcium phosphate (TCP) powder for the printing process was described previously [5]. Briefly, an equimolar mixture of di-calcium phosphate anhydrous (DCPA, $CaHPO_4$, monetite) and calcium carbonate (both Merck, Darmstadt, Germany) was heated to a temperature of 1400 °C for a period of 5 h followed by quenching to room temperature. The sintered cake was crushed with a pestle and mortar and sieved through 160 µm pores. The 3D printing of cement scaffolds was performed with a multi-color 3D-powder printing system (spectrum Z510, Z-Corporation, USA) using powder and a binder solution of 20% phosphoric acid (Merck, Darmstadt, Germany). The layer thickness was chosen to 125 µm. The binder-volume ratio corresponded to 0.371.

Subsequent to the printing, the tri-calcium phosphate scaffolds were manually taken out the powder bed. The individual scaffolds were rotated to eliminate the non-bonded powder. Nevertheless, a significant amount of the powder particles remained inside the micro-pores. Before any post-printing treatment can be performed, which includes the application of phosphoric acid to stabilize the 3D construct and in due course etch to widen the micro-pores, the tri-calcium phosphate that closes pores has to be removed.

The removal of tri-calcium phosphate particles captured in the pores of the scaffold was more complicated than originally expected. Therefore, vacua, air jets and the combinations of both were applied. Finally, the particles were removed using compressed air (AC 200 Smile Oelfrei, Switzerland) through a 15 gauge needle. The applied pressure was set between 6 and 9 bar.

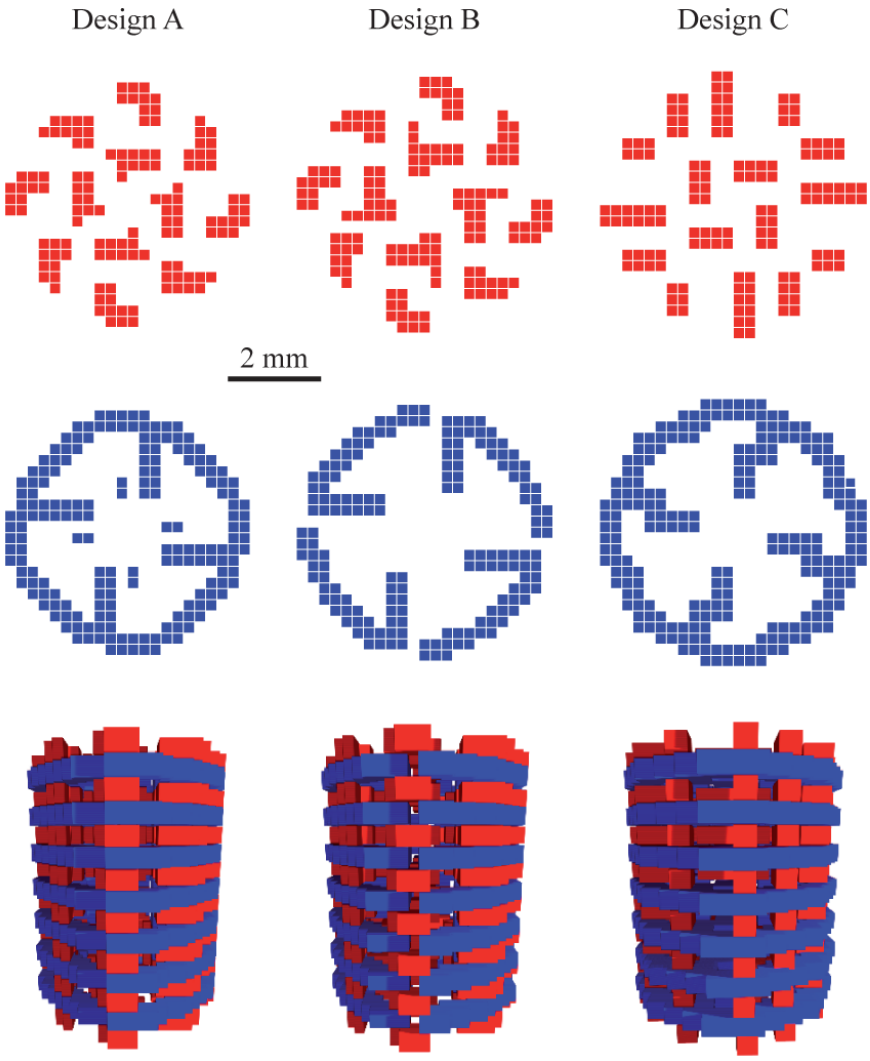

Fig. 1. The scaffolds consist of 15 alternating layers shown in red and blue, respectively. The entire construct resembles long bone architectures with the porous inner part and the more compact outer part that provides the mechanical stability.

2.3 3D imaging of biomimetic bone scaffolds using micro computed tomography

Conventional micro computed tomography (μCT) served for the visualization of the different tri-calcium phosphate scaffolds. Three scaffolds of each design and each scaling factor (100%, 125%, 150%, 175% and 200%) were scanned using the system SkyScan 1174™ (Skyscan, Kontich, Belgium) with an acceleration voltage of 50 keV and a beam current of 800 μA (in total 45 scans). Each scan consisted of 900 projections taken over 360°. A 0.5 mm-thick aluminum filter was applied to increase the mean X-ray energy. Adapted to specimen diameter, the isotropic pixel size ranged from 17 μm to 32 μm. The acquired projections of 1024 × 1024 pixels were incorporated into a modified Feldkamp algorithm using the SkyScan Nrecon™ software to non-destructively generate the three-dimensional tomography data.

Synchrotron radiation-based μCT at the beamline W2 (HASYLAB at DESY, Hamburg, Germany), a synchrotron radiation source of the second generation was carried out using the standard set-up for absorption contrast that is operated by the GKSS Research Center [14]. Three scaffolds (100%) of Design A, B and C were measured at a photon energy of 30 keV to approximately reach the total absorption of 2. Because of the parallel X-rays, the specimens were only measured over 180° in steps of 0.25° (720 projections) at two height levels combined after reconstruction with voxel resolution [12]. The selected optical magnification of 2.18 resulted in an isotropic effective voxel size of 4.12 μm. The spatial resolution determined on the basis of the 10% value of the modulated transfer function [15] corresponded to 8.05 μm. In addition, five scaffolds of Design A (scaling 100%, 125%, 150%, 175%, and 200%) were acquired using a

photon energy of 36 keV with a pixel size of 4.15 µm and a spatial resolution of 8.8 µm. Here, an asymmetric sample rotation with 360° rotation (angular steps 0.25°) [16] were applied to get a similar spatial resolution as for the 100% scaffolds. Data reconstruction was based on the back-projection of filtered projections (BKFIL-algorithm) [17].

Commercially available software was applied for the 3D visualization of the scaffolds (VG Studio Max 1.2.1, Volume Graphics, Heidelberg, Germany). For the quantitative evaluation of the tomography data, dedicated software was developed using IDL 7 (ITT Visual Information Solutions, Boulder, CO, USA).

2.4 Cell experiments on 3D bone scaffolds

The 3D hydroxy apatite scaffolds were seeded with human multi-potent dental neural crest-derived progenitor cells (dNC-PCs) and cultured for a period of 28 d either in growth medium or in osteogenic medium. The exact seeding and culturing procedure has been described previously [12, 18]. For immunohistochemistry, the samples were decalcified with 10% ethylenediaminetetraacetic acid (VWR, Darmstadt, Germany) in Tris buffered saline for 7 d, embedded into paraffin and subsequently sectioned (HM 355 S; Microm International GmbH, Walldorf, Germany). The paraffin sections were immunostained with mouse anti-human osteocalcin antibody (1:200; Acris, Hiddenhausen, Germany) and with mouse anti-human alkaline phosphatase antibody (1:200; Biogenesis, Oxford, UK). Immunoperoxidase labeling was performed using diaminobenzidine precipitation for detection (R&D, Minneapolis MN, USA).

For the non-decalcified sections of the cell-seeded scaffolds, the dNC-PCs were again fixed in 4% paraformaldehyde. After careful embedding and complete polymerization in Technovit 9100 New (Heraeus-Kulzer, Hanau, Germany), 5 µm thin sections were prepared using the RM 2155 microtome (Leica, Bensheim, Germany). Before staining, the slices were deacrylated twice in xylol for a period of 15 min and 2-methoxyethylacetate for a period of 10 min each. The clearing procedure included decreasing ethanol series (two times isopropyl alcohol, two times 96% ethanol, two times 70% ethanol, for a period of 2 min each) followed by re-hydration to distilled water. For the staining the re-hydrated slices were incubated in 0.1% toluidine blue O (Sigma, Seelze, Germany) for a period of 20 s, washed in distilled water, dehydrated in ethanol, and mounted in Eukitt (Labonord, Mönchengladbach, Germany). Optical micrographs were obtained with a Zeiss Axioskop 40 or a Zeiss Imager Z1 microscope equipped with a scanning stage, both combined with a Zeiss AxioCam Mrc digital camera and Zeiss AxioVision software (Oberkochen, Germany).

3. RESULTS

3.1 Tomographic imaging with micrometer resolution

Opaque scaffolds as fabricated from different kinds of calcium phosphates should exhibit a porous structure that permits cell attachment and migration. The cavities in the scaffold should provide minimal diameters of 100 µm or more in order to promote the cell in-growth. Therefore, micro computed tomography with a spatial resolution between 1 and 10 µm is well suited for the quantification of the micrometer-wide pores.

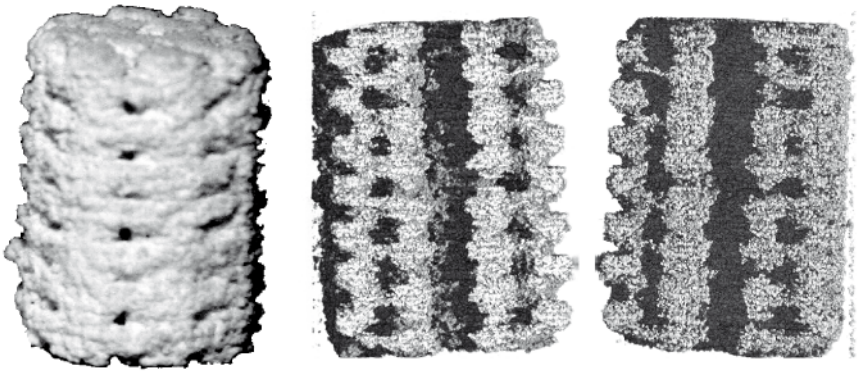

Fig. 2. The photograph (left image) only gives an impression of the scaffold's outer surface, since the calcium phosphate 3D-printed scaffolds with central channel are opaque. The tomography data allow for any desired virtual cut through the scaffold. For example, one can identify numerous loosely bonded particles, which were impossible to be removed from the micro-channels.

Figure 2 elucidates the gain of information comparing optical images of the opaque tri-calcium phosphate scaffolds (photograph on the left side) with tomography data that allow for the visualization of any virtual cut through the three-dimensional data. Hence, tomography gives rise to the wealth of pore structures on the micrometer level. It is especially supportive to measure the diameter of the central canal, where the optical image just gives a lower limit.

At first glance, one recognizes in the tomography data smaller pores that expected from Design A. This impression becomes clearer in Figure 3. It shows the comparison between two selected tomography slices and the manually overlaid layers of Design A. On the one hand, the red-colored design slices are significantly smaller than the representation of the calcium phosphate. The pores, on the other hand, are much smaller than designed.

The visual inspection of the tomography data uncovers the presence of loosely bonded particles in the micro-passages, which even closes several of the pores. The slices in Figure 3 indicates that the smaller the pores the more probable the presence of filled micro-passages. Size and shape of the particles seem to be sub-optimal for the realization of the scaffolds. Therefore, larger scaffolds with scaling factors of 125%, 150%, 175%, and 200% have been built to get an idea at which diameters the micro-pores are not closed anymore. Figure 4 shows the results for Design A scaffolds, which were obtained by conventional micro computed tomography. Although the general quality is improving towards the higher scaling factors, even the 200% scaffold exhibits noteworthy deficiencies in relation to the designed structure.

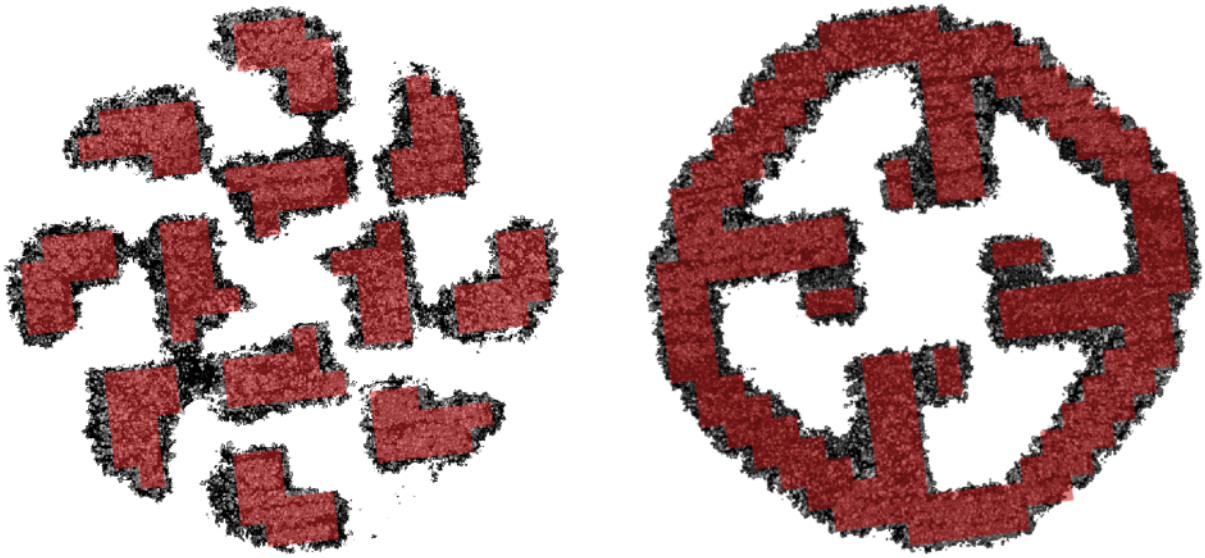

Fig. 3. The manually registered slices (synchrotron-radiation-based micro computed tomography with the Design A) show the close similarity between design and 3D-printed TCP scaffold. The fabricated scaffold, however, exhibits a significantly larger volume. Unfortunately, the smaller pores are filled with particles.

Compared to the hydroxy apatite scaffolds (cp. Figure 5), the tri-calcium phosphate constructs are less filigree, which might prevent an effective accessibility of the cells. An approach to determine the accessibility by means of computer simulations is given in Figure 5. Virtual hard spheres of increasing diameter were allowed moving through the micro-passages uncovered by the tomography of the scaffold to determine the accessible volume of the porous network.

Spheres with diameters of up to 320 µm can reach more than 50% of the interconnected pores, whereas spheres with diameters above 350 µm do not reach the central part of the hydroxy apatite scaffolds. Hence, the computer simulations allow extracting a meaningful parameter for the accessibility of the entire scaffold by migrating cells of choice.

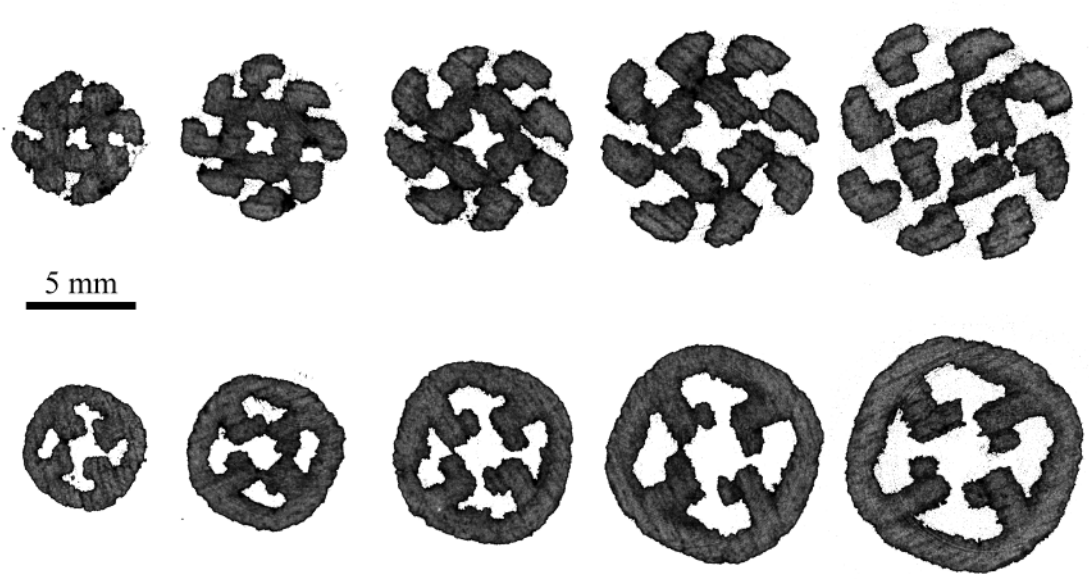

Fig. 4. The slices of the two different layers of Design A are selected from scaled scaffolds that were acquired by means of conventional micro computed tomography (SkyScan 1174™). From left to right, the scaling factor corresponds to 100%, 125%, 150%, 175%, and 200%. The details and the improved accessibility for larger scaling factors can be clearly identified.

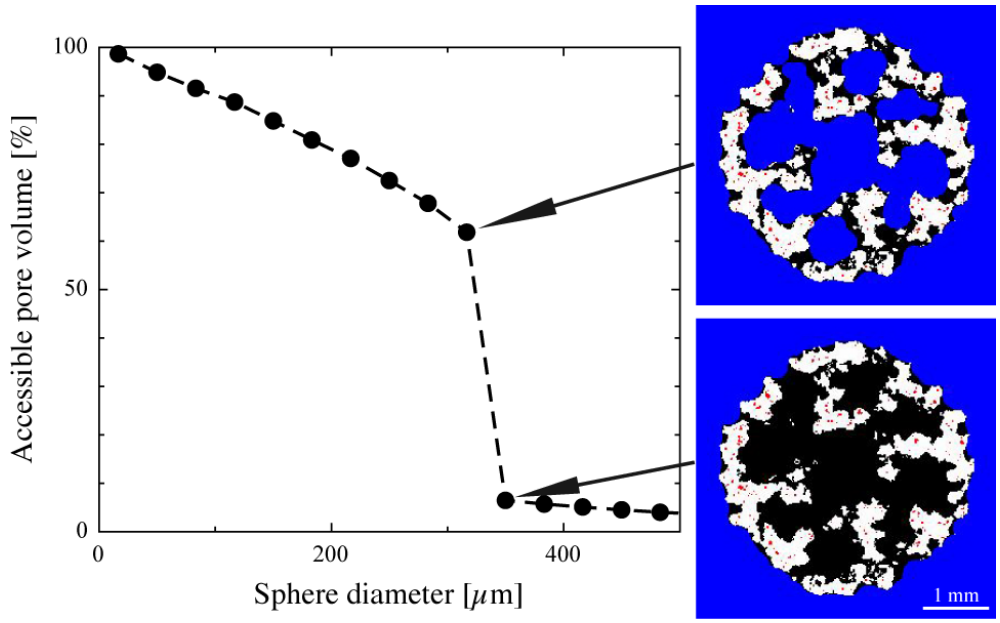

Fig. 5. The hydroxy apatite scaffold Design A is accessible via its micro-channels for spheres with a diameter of about 350 µm. Such a large value is high enough for cell in-growth and capillary formation. The colors of the selected slices represent the material (white), the accessible volume (blue), the inaccessible parts (black) and the closed pores (red).

3.2 Mechanical characterization of the tri-calcium phosphate scaffolds

The sintered hydroxyapatite scaffolds made out of the porous spray-dried hollow spheres are so fragile that a meaningful mechanical characterization is inappropriate. We only realized differences in the mechanical properties during manual handling. Design B yielded the most fragile scaffolds.

It should be mentioned that the mechanical properties of the hydroxy apatite scaffolds become better by the cell seeding. Nevertheless, the improvement is restricted, so that significant evolution is only achieved by modified fabrication procedures.

The tri-calcium phosphate scaffolds reach much better mechanical stabilities that allow for the quantification of the bare constructs. The preparation procedures should be optimized to reach the mechanical properties of bony tissues. For this optimization, preliminary mechanical testing is very supportive. The stress-strain curve in Figure 6 belongs to these preliminary compression tests performed for different scaffold designs and scaling factors.

The Young's moduli of the tri-calcium phosphate scaffolds have been determined from the linear fits within the initial stages of loading as indicated in Figure 6. The applied uni-axial scaffold deformation of 1 mm/min results in compressive load, which was measured with a 2 kN load cell of the universal testing machine (D020, Zwick GmbH&Co. KG, Ulm, Germany). Figure 6 exhibits the stress-strain behavior that includes characteristic steps. One can observe increasing strains at rather constant stresses.

The tri-calcium phosphate scaffolds have a Young's modulus that is about three orders of magnitude smaller than that of the healthy human tibial cortical bone [19]. Although the individual measurements can be performed with high accuracy, the data from scaffold to scaffold vary much more than for typical engineered materials. The mean values of the different designs, however, follow the qualitative impression from the hydroxy apatite scaffolds: Design B is mechanically less stable than the other two designs (cp. Table 1). The experimental data presented in Table 1 also indicate that scaffolds scaled to larger sizes exhibit better mechanical properties. The restricted number of experiments, however, does not allow any statistically relevant conclusion.

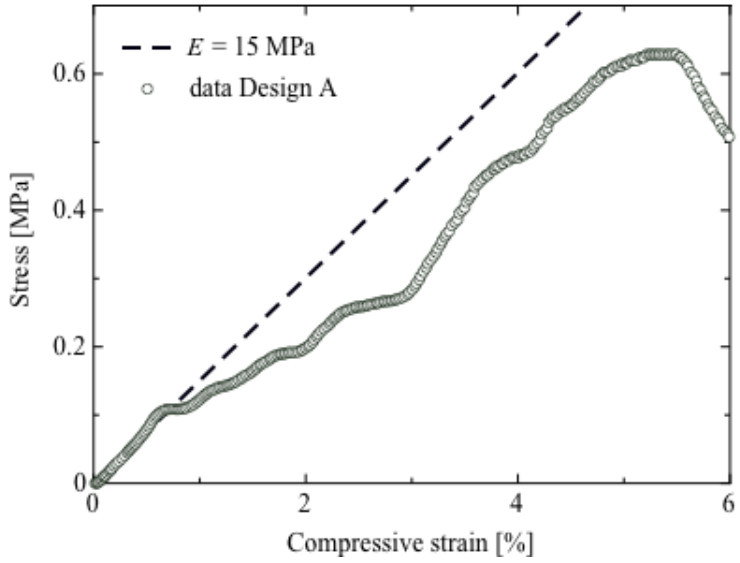

Fig. 6. The typical stress-strain curves of the tri-calcium phosphate scaffolds contain steps that correspond to the cracking of individual layers. The empty circles represent the measured data. The dotted line is the linear fit of the initial stages to characterize the Young's modulus of the selected scaffold.

Table. 1. The Young's moduli of the tri-calcium phosphate scaffolds (Designs A, B, C) significantly scatter indicating some difficulties in the reproducible scaffold preparation.

Scaffold	Length/mm	Diameter/mm	Weight/g	Young's modulus/MPa
A1	7.4	5.4	0.173	21.2 ± 0.4
A2	7.4	5.5	0.170	35.7 ± 0.2
A3	7.5	5.4	0.167	17.6 ± 0.2
A4	7.4	5.4	0.167	38.8 ± 0.4
A5	7.4	5.4	0.161	15.0 ± 0.3
A6	7.4	5.4	0.154	32.8 ± 0.2
A				$\langle E_A \rangle$ **27 ± 4**
A 125%	9.3	6.7	0.325	58.0 ± 0.3
A1 150%	11.2	8.0	0.550	31.4 ± 0.8
A2 150%	11.2	8.0	0.550	57.2 ± 0.8
A1 175%	12.9	9.3	0.817	40.4 ± 0.4
A2 175%	13.0	9.3	0.828	51.6 ± 0.5
B1	7.5	5.7	0.174	19.5 ± 0.4
B2	7.5	5.7	0.181	17.4 ± 0.4
B3	7.5	5.7	0.164	18.0 ± 0.4
B4	7.5	5.6	0.163	21.1 ± 0.5
B5	7.5	5.7	0.164	23.1 ± 0.4
B				$\langle E_B \rangle$ **20 ± 1**
C1	7.5	6.2	0.193	29.3 ± 0.1
C2	7.5	6.3	0.198	28.2 ± 0.4
C3	7.5	6.1	0.188	31.3 ± 0.8
C4	7.5	6.1	0.196	19.4 ± 0.2
C5	7.5	6.1	0.213	49.8 ± 0.4
C				$\langle E_C \rangle$ **32 ± 5**

3.3 Cyto-compatibility of the hydroxy apatite scaffolds

Cell seeding is usually beneficial, since the cell-seeded construct will show improved mechanical properties with respect to the bare ceramic scaffold. It is, therefore, the aim to obtain a homogeneously seeded scaffold, which is rather difficult to obtain and to verify [12]. Usually the bony tissues are de-calcified for histological sectioning. This is, however, not helpful here, because the printed structure will collapse and the relation to the individual design becomes impossible. The cutting of the non-de-calcified specimen is demanding, but as shown by the histological image in Figure 7 achievable. Figure 7 reveals the ceramic parts in light gray as well as the cells. The original design is overlaid in order to show the degree of (dis-)similarity.

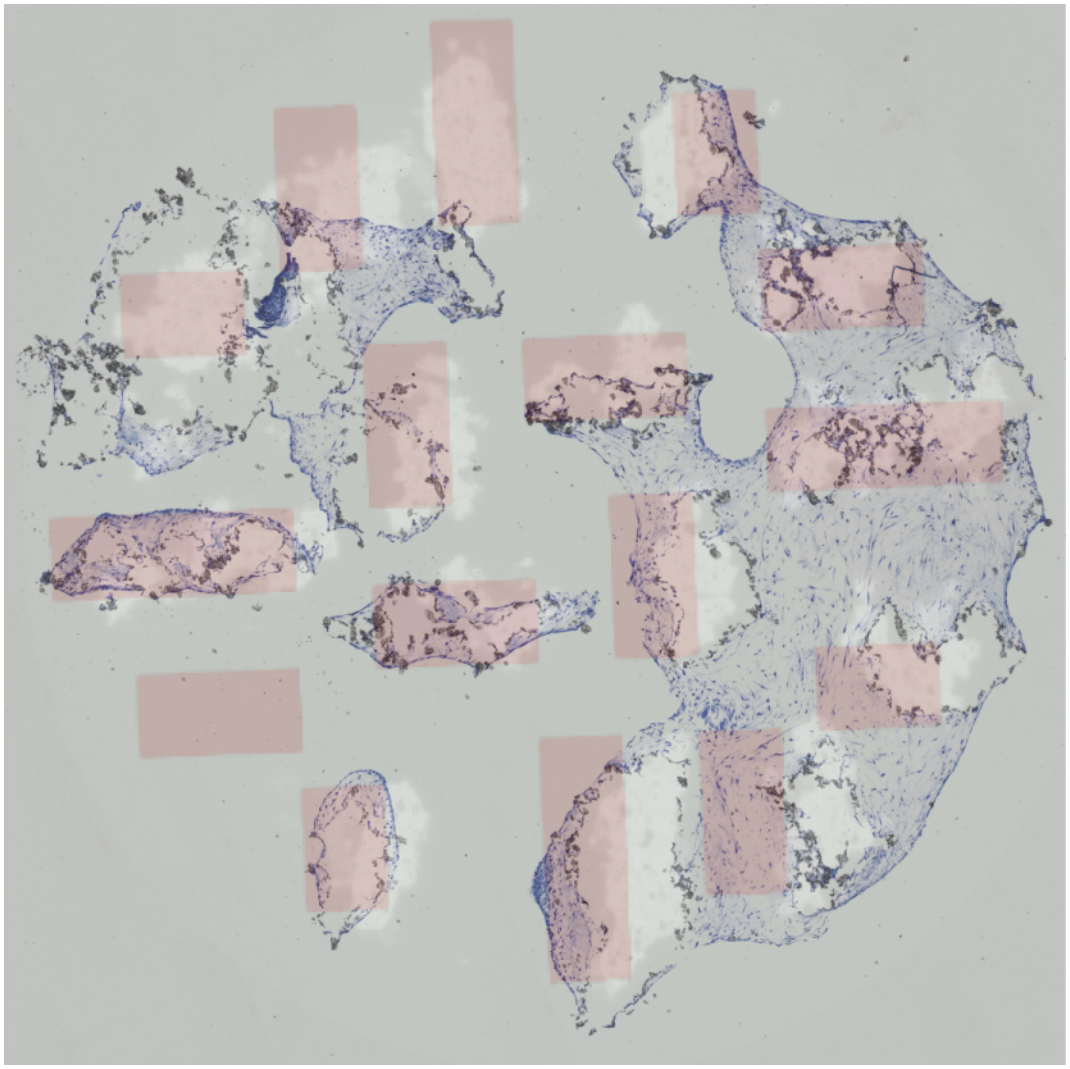

Fig. 7. The tomography data of a hydroxy apatite scaffold (Design C) in light gray are manually superimposed to the non-de-calcified section with toluidine blue stained cells. For comparison, Design C is overlaid in light red. The image shows the cell distribution that reaches the center of the scaffold.

As shown by SEM micrographs in Figure 8, the cells were attached to the nano-porous hydroxy apatite granules in a healthy shape. The upper image gives an impression of a cell covering several granules. For a more detailed investigation the selected area marked by the yellow-colored square was milled using a focused beam of gallium ions. The lower SEM-image of Figure 8 shows a detailed image of the milled cross section. In the upper part of the image, one finds the cell that was covered by 15 nm-thin gold coating to ensure sufficient electrical conductivity for the successful electron microscopy imaging. On the left, the hydroxy apatite granule has a pore indicating the internal porosity resulting from the spray-drying process. The grain structure can straightforwardly be seen in the uncovered granule in the right half of the image above the scale bar.

The cell layer with a thickness between 220 and 550 nm can be clearly recognized on top of the granule. No structural details are visible within the cell layer since staining to enhance contrast was avoided. Nevertheless, the excellent attachment of the cell to the ceramic surface, proven by the in-growth of the cell into the open surface pores of the granule, points out the cyto-compatibility of the 3D-printed hydroxy apatite scaffold.

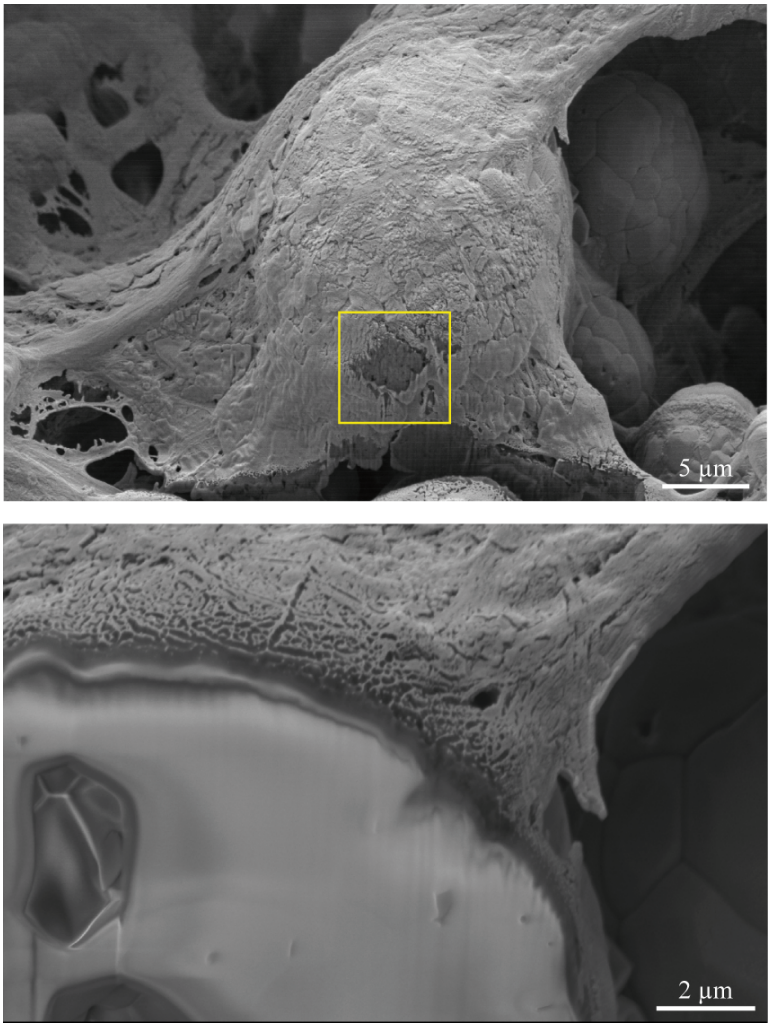

Fig. 8. The SEM micrographs show a cell-covered hydroxy apatite granule. The upper image gives an overview of a selected hydroxy apatite granule of the scaffold, completely covered by a cell. The yellow square marks the region of interest, which was milled for a cross-sectional investigation using the focused Ga-ion beam. The lower SEM image is a more detailed view of the granule after the ion milling.

4. DISCUSSION

Rapid prototyping (3D-printing) belongs to promising preparation routes to fabricate patient-specific bone replacements. Combining nano-porous granules and micrometer-precise printing, macroscopic scaffolds with designed architecture down to the molecular level are realized. The nano-porosity can be tailored adapting the parameters during spray drying and sintering. The morphological parameters of the granules, that means morphology, average size and size distribution, as well as amount and nature of the binder give rise to the characteristic packaging and related nano-pores and smaller micro-pores.

The flexibility of the method allows fabricating more complex architectures than for instance by needle insertion [20], where only straight micro-channels can be made. The main restriction of 3D-printing lies in the achievable voxel size. Therefore, nanometer-sized pores are only mean values with an inherent size distribution and cannot be chosen individually. This is the reason, why micro computed tomography is perfectly suited for the morphological characterization. It includes the conversion of X-rays to light. Without any X-ray optics, the spatial resolution of micro computed tomography is generally restricted to the micrometer scale. There exist high-resolution systems that reach several hundred nanometers, but which also do not support the pore quantification on the nanometer scale.

For the quantitative characterization of the micrometer-sized pores micro computed tomography is a powerful tool. Qualitative conclusions can be drawn from simple visual inspection and manual registration. Although the quantitative evaluation requires sophisticated software to treat the large datasets of GB size such a careful and detailed analysis of the porous structures allows extracting important parameters for their behavior in biological environment. The incorporation as bone implant requires reasonably high mechanical stability. Superior mechanical properties, however, mean less porous scaffolds. Consequently, the challenge corresponds to an optimization task and the mechanics of the 3D-printed constructs has to be measured. The preliminary results presented here are promising, but also demonstrate that the irregular structure of cancellous or spongy bone might be the better choice with respect to the bi-layer design used. For example, the observed steps in the stress-strain curves can be simply interpreted as a successive braking of the scaffold layers that are arranged perpendicular to the compressive loading. Nature-inspired bone scaffolds for load-bearing implants need the deeper understanding of the healthy trabecular bone.

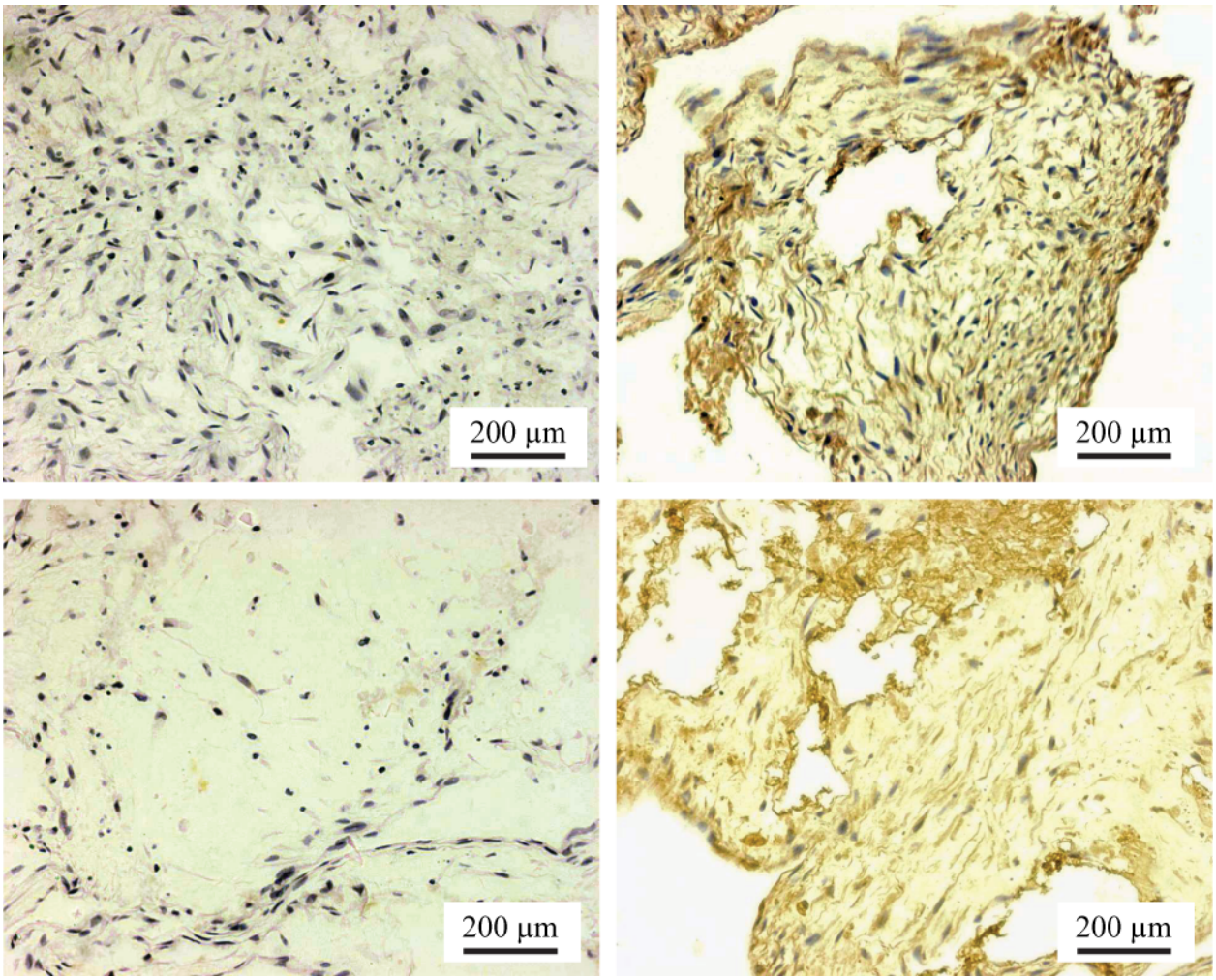

Fig. 9. The immunohistochemical analysis provides evidence for the osteogenic differentiation of dNC-PCs seeded onto HA scaffolds and cultured in osteogenic medium for 28 d. ALP (top-right image) and OC stains (bottom-right image) both exhibit positive signals in contrast to the corresponding negative controls (left images).

The mechanical properties of the tri-calcium phosphate scaffolds can be further improved applying additional phosphoric acid applications [5, 21]. Such post-processing is under investigation and comprises dip and spray treatments. Higher doses lead to etching and reduced mechanical stabilities. It is, however, a route to increase the mean pore diameters, if desired. Such treatments do not only alter the morphological and mechanical characteristics but may have a negative influence on cell behavior because of significant differences of the pH-value from physiological conditions. Hence,

further processing of the calcium phosphate structures are expected to reach cyto-compatibility as demonstrated for the hydroxy apatite microstructures.

The non-de-calcified sections verify the cell distribution within the entire scaffold. Their preparation, however, is problematical and often without success. Decalcified sections allow for the immunohistochemical analysis. The cells cultured in osteogenic stimulation medium stained positive for osteocalcin, an osteogenic differentiation marker, while the cells cultured in osteogenic stimulation medium as well as in simple growth medium exhibited positive signals of alkaline phosphatase. The cyto-compatibility of 3D-printed brushite [22] and hydroxy apatite scaffolds [23] was previously demonstrated. Currently, the differentiation of dNC-PCs into bone producing cells has been established in vitro and in vivo [18]. In this 3D-culture system, the expression of osteocalcin pointed out the dNC-PCs osteogenic differentiation. Thus, the immunohistochemical analyses exhibited positive signals and desired cell behavior as exemplary shown by the images in Figure 9. The osteogenic differentiation of the cells seeded on the 3D-printed scaffolds is demonstrated by both the alkaline phosphatase and osteocalcin activities. This behavior is not surprising as hydroxy apatite is the main inorganic component of human bone. Unfortunately, the materials sintered at temperatures above 1000 °C contain less water than the hydroxy apatite from biomineralization processes and cannot be incorporated in the remodeling. Therefore, alternative procedures, which are performed at ambient temperatures such as the cement approach, are worth being investigated in some detail.

3D-printers and nano-porous granules or powders are the basis to fabricate scaffolds that are step-wise improved according to biomimetic design rules. After appropriate cell seeding these nature-inspired structures composed of man-made and biological components should become available to fill patient-specific cavities and take over the mechanical load. In this way, engineers can successfully contribute to emerging technologies in life sciences including tissue engineering and regenerative medicine, which finally results in benefits for patients.

REFERENCES

[1] C. X. F. Lam, X. M. Mo, S. H. Teoh *et al.*, "Scaffold development using 3D printing with a starch-based polymer," Mat. Sci. Eng. 20, 49-56 (2002).

[2] R. Lowmunkong, T. Sohmura, J. Takahashi *et al.*, "Transformation of 3DP gypsum model to HA by treating in ammonium phosphate solution," J. Biomed. Mater. Res. B Appl. Biomater. 80, 386-393 (2007).

[3] R. A. Giordano, B. M. Wu, S. W. Borland *et al.*, "Mechanical properties of dense polylactic acid structures fabricated by three dimensional printing," J. Biomater. Sci. Polym. Ed. 8, 63-75 (1996).

[4] W. Huang, Q. Zheng, W. Sun *et al.*, "Levofloxacin implants with predefined microstructure fabricated by three-dimensional printing technique," Int. J. Pharm. 339, 33-38 (2007).

[5] U. Gbureck, T. Hölzel, C. Doillon *et al.*, "Direct printing of bioceramic implants with spatially localised angiogenic factors," Adv. Mater. 19, 795-800 (2007).

[6] A. Khalyfa, S. Vogt, J. Weisser *et al.*, "Development of a new calcium phosphate powder-binder system for the 3D printing of patient specific implants," J. Mater. Sci. Mater. Med. 18, 909-916 (2007).

[7] B. Leukers, H. Gulkan, S. H. Irsen *et al.*, "Hydroxyapatite scaffolds for bone tissue engineering made by 3D printing," J. Mater. Sci. Mater. Med. 16, 1121-1124 (2005).

[8] R. Chumnanklang, T. Panyathanmaporn, K. Sitthiseripratip *et al.*, "3D printing of hydroxyapatite: Effect of binder concentration in pre-coated particle on part strength," Mat. Sci. Eng. C27, 914-921 (2007).

[9] H. Seitz, W. Rieder, S. Irsen *et al.*, "Three-dimensional printing of porous ceramic scaffolds for bone tissue engineering," J. Biomed. Mater. Res. Part B: Appl. Biomater. 74, 782-788 (2005).

[10] J. E. Barralet, K. J. Lilley, L. M. Grover *et al.*, "Cements from nanocrystalline hydroxyapatite," J. Mater. Sci. Mater. Med. 15, 407-411 (2004).

[11] J. E. Barralet, M. J. Tremayne, K. J. Lilley *et al.*, "Chemical modification of calcium phosphate cements with hydroxy acids and their salts," Chem. Mater. 17, 1313-1319 (2005).

[12] F. C. Fierz, F. Beckmann, M. Huser *et al.*, "The morphology of anisotropic 3D-printed hydroxyapatite scaffolds," Biomaterials 29, 3799-3806 (2008).

[13] S. H. Irsen, B. Leukers, C. Hockling *et al.*, "Bioceramic granulates for use in 3D printing: Process engineering aspects," Materialwissenschaft und Werkstofftechnik 37, 533-537 (2006).

[14] F. Beckmann, "Microtomography using synchrotron radiation as a user experiment at beamlines BW2 and BW5 of HASYLAB at DESY," Proc. SPIE 4503, 34-41.

[15] B. Müller, P. Thurner, F. Beckmann *et al.*, "Non-destructive three-dimensional evaluation of biocompatible materials by microtomography using synchrotron radiation," Proc. SPIE 4503, 178-188.
[16] B. Müller, R. Bernhardt, T. Weitkamp *et al.*, "Morphology of bony tissues and implants uncovered by high-resolution tomographic imaging," Int. J. Mat. Res. 98, 613-621 (2007).
[17] A. C. Kak, and M. Slaney, [Principles of Computerized Tomographic Imaging] IEEE Press, New York(1988).
[18] O. Degistirici, C. Jaquiery, B. Schoenebeck *et al.*, "Defining Properties of neural Crest-Derived Progenitor Cells from the Apex of Human Developing Tooth," Tissue Engineering: Part A 14, 317-330 (2008).
[19] B. K. Hoffmeister, S. R. Smith, S. M. Handley *et al.*, "Anisotropy of Young's modulus of human tibial cortical bone," Med. Biol. Eng. Comput. 38, 333-338 (2000).
[20] F. R. Rose, L. A. Cyster, D. M. Grant *et al.*, "In vitro assessment of cell penetration into porous hydroxyapatite scaffolds with a central aligned channel," Biomaterials 25, 5507-5514 (2004).
[21] U. Geburek, T. Hölzel, U. Klammert *et al.*, "Resorbable dicalcium phosphate bone substitutes made by 3D powder printing," Adv. Func. Mater. 17, 3940-3945 (2007).
[22] U. Klammert, T. Reuther, C. Jahn *et al.*, "Cytocompatibility of brushite and monetite cell culture scaffolds made by three-dimensional powder printing," Acta Biomaterialia 5, 727-734 (2009).
[23] B. Leukers, H. Gulkan, S. Irsen *et al.*, "Biocompatibility of ceramic scaffolds for bone replacement made by 3D printing," Materialwissenschaft und Werkstofftechnik 36, 781-787 (2005).